Acta Crystallographica Section D
Biological Crystallography
ISSN 1399-0047

Atomic resolution crystal structure of glutaredoxin 1 from *Plasmodium falciparum* and comparison with other glutaredoxins

Manickam Yogavel,[a] Timir Tripathi,[b] Ankita Gupta,[b] Mudassir Meraj Banday,[a] Stefan Rahlfs,[c] Katja Becker,[c] Hassan Belrhali[d,e] and Amit Sharma[a]*

[a]Structural and Computational Biology Group, International Centre for Genetic Engineering and Biotechnology (ICGEB), Aruna Asaf Ali Road, New Delhi 110 067, India, [b]Department of Biochemistry, North-Eastern Hill University, Shillong 792 022, India, [c]Biochemistry and Molecular Biology, Interdisciplinary Research Center, Justus Liebig University Giessen, 35392 Giessen, Germany, [d]European Molecular Biology Laboratory, 6 Rue Jules Horowitz, BP 181, 38042 Grenoble, France, and [e]Unit for Virus Host-Cell Interactions, University Grenoble Alpes-EMBL-CNRS, 6 rue Jules Horowitz, 38042 France

Correspondence e-mail: amit.icgeb@gmail.com

Received 28 June 2013
Accepted 11 September 2013

PDB References: glutaredoxin 1, 4hjm; 4kje; 4kjf

Glutaredoxins (Grxs) are redox proteins that use glutathione ($^{\gamma}$Glu-Cys-Gly; GSH) as a cofactor. *Plasmodium falciparum* has one classic dithiol (C*XX*C) glutaredoxin (glutaredoxin 1; PfGrx1) and three monothiol (C*XX*S) Grx-like proteins (GLPs), which have five residue insertions prior to the active-site Cys. Here, the crystal structure of PfGrx1 has been determined by the sulfur single-wavelength anomalous diffraction (S-SAD) method utilizing intrinsic protein and solvent S atoms. Several residues were modelled with alternate conformations, and an alternate position was refined for the active-site Cys29 owing to radiation damage. The GSH-binding site is occupied by water polygons and buffer molecules. Structural comparison of PfGrx1 with other Grxs and Grx-like proteins revealed that the GSH-binding motifs (C*XX*C/C*XX*S, TVP, CDD, Lys26 and Gln/Arg63) are structurally conserved. Both the monothiol and dithiol Grxs possess three conserved water molecules; two of these were located in the GSH-binding site. PfGrx1 has several polar and charged amino-acid substitutions that provide structurally important additional hydrogen bonds and salt bridges missing in other Grxs.

1. Introduction

The intracellular redox milieu influences cellular functions, including those of gene expression, DNA synthesis, apoptosis and cellular signalling. Glutaredoxins (Grxs) are a family of small thiol–disulfide oxidoreductases that are ubiquitous and conserved in evolution. They are involved in the maintenance of thiol–disulfide redox equilibrium within cells (Fernandes & Holmgren, 2004; Holmgren *et al.*, 2005; Lillig *et al.*, 2008) and utilize electrons provided by the tripeptide glutathione ($^{\gamma}$Glu-Cys-Gly; GSH) to catalyze thiol–disulfide exchange reactions. Structurally, all Grxs share a common topological fold, the thioredoxin fold, which consists of four-stranded β-sheets flanked by three to five α-helices. Grxs were discovered as GSH-dependent hydrogen donors for ribonucleotide reductase in an *Escherichia coli* mutant lacking Trxs (Holmgren, 1976). Since then, Grxs have been assigned several other functions such as the reduction of methionine sulfoxides and sulfates (Gonzalez Porqué *et al.*, 1970; Tsang, 1981). Grxs act as general thiol–disulfide oxidoreductases and help to protect cells against oxidative stress by detoxifying oxidizing agents (Holmgren, 1979, 2000; Axelsson & Mannervik, 1980). Grxs are also involved in regulating transcription-factor binding activity (Matthews *et al.*, 1992; Pineda-Molina *et al.*, 2001),

apoptosis (Chrestensen *et al.*, 2000), redox-signal transduction and protein translocation (Shelton *et al.*, 2005). Grxs catalyze important steps in oxidative protein folding by making protein–protein interactions and conducting covalent catalysis to act as chaperones and isomerases of disulfides (Berndt *et al.*, 2008). Several Grxs bind to Fe–S clusters both *in vitro* and *in vivo*, thereby helping in intracellular iron sensing, electron transfer, enzyme catalysis and regulation (Lillig *et al.*, 2005; Feng *et al.*, 2006; Lill *et al.*, 2006; Iwema *et al.*, 2009; Hoff *et al.*, 2009; Mühlenhoff *et al.*, 2010). The functionally and mechanistically heterogeneous class of Grxs can be subdivided into monothiol (C*XX*S) and dithiol (C*XX*C) Grxs depending on the number of cysteine residues present in the active site. In parallel to this, two distinct mechanisms have been proposed to explain Grx activity based on one or two active-site cysteines. In the monothiol mechanism, only the N-terminal cysteine is required for reduction of Grx–GSH mixed disulfides, while in the dithiol mechanism Grxs can reduce both low-molecular-weight ligands and protein disulfides using both active-site cysteines (Fernandes & Holmgren, 2004; Gallogly *et al.*, 2009). Both pathways use GSH as a reductant and concomitantly produce GSSG, which is in turn reduced back to GSH *via* glutathione reductase (GR) and NADPH.

Besides having three monothiol Grx-like proteins (GLPs), *Plasmodium falciparum* harbours a single gene encoding a typical dithiol Grx (PfGrx1), which is cytoplasmic (Rahlfs *et al.*, 2001; Kehr *et al.*, 2010). PfGrx1 displays glutathione:HEDS activity and can reduce ribonucleotide reductase and the thioredoxin-like protein plasmoredoxin *in vitro* (Rahlfs *et al.*, 2001). PfGrx1 is highly thermostable and resistant to denaturants and pH changes (Tripathi *et al.*, 2010). Several studies have identified interactions between Grxs and their partner proteins in plants, eukaryotic parasites and other organisms (Motohashi *et al.*, 2001; Lindahl & Florencio, 2003; Balmer *et al.*, 2003; Lemaire *et al.*, 2004; Wong *et al.*, 2004; Rouhier *et al.*, 2005; Sturm *et al.*, 2009). These interacting proteins are involved in many processes, including oxidative stress response (peroxiredoxins, ascorbate peroxidase and catalase), carbon/nitrogen/sulfur metabolism (*S*-adenosylmethionine synthetase, *S*-adenosyl-L-homocysteine hydrolase and phosphoglycerate kinase), protein biosynthesis (elongation factors) and protein folding (heat-shock proteins and protein disulfide isomerase). Recently, it has been shown that the parasite *P. falciparum* antioxidant protein (PfAOP; 1-Cys peroxiredoxin) requires PfGrx1 and glutathione as substrates for the reduction of hydroperoxides (Djuika *et al.*, 2013). In this work, we provide atomic resolution structural information on PfGrx1. The latter has several additional hydrogen bonds and salt bridges owing to polar and charged amino-acid substitutions when compared with other Grxs. PfGrx1 has a unique hydrophobic pocket filled with the crystallization solvent molecule MPD. We also show that the disulfide bond between Cys29 and Cys32 is broken up on exposure to synchrotron radiation. Finally, our analysis of residue conservation and surface electrostatic potential distributions in Grxs provides insights into the intriguing structural diversity of Grxs.

2. Materials and methods

2.1. Expression and purification of the recombinant protein

Recombinant PfGrx1 was produced as described by Rahlfs *et al.* (2001). *Escherichia coli* M15 cells were transformed with the respective pQE30*grx* plasmid. 5 ml of LB medium was inoculated with a single colony and used as a starter culture for a 500 ml culture. The cells were grown at 310 K in LB medium containing ampicillin (100 µg ml^{-1}) and kanamycin (50 µg ml^{-1}) to an A_{600} of 0.6; subsequently, protein expression was induced by adding 1 m*M* isopropyl β-D-1-thiogalactopyranoside (IPTG). The cells were grown for an additional 4 h, harvested, and either directly used for protein purification or frozen at 253 K. For purification, bacterial cells were disintegrated *via* sonication in the presence of a protease-inhibitor cocktail. The protein was purified using Ni^{2+}–NTA beads (Qiagen) and gel-filtration chromatography. Fractions containing the protein were analyzed by SDS–PAGE (Supplementary Fig. S1[1]). The purified protein was finally concentrated and the buffer was exchanged to 50 m*M* HEPES, 50 m*M* KCl, 1 m*M* EDTA pH 8.0.

2.2. Crystallization, sulfur-SAD and atomic resolution data collection

Crystallization experiments were performed using the hanging-drop vapour-diffusion method at 293 K. Initial crystallization screening was carried out in a Costar 96-well tissue-culture plate (Corning, Lowell, Massachusetts, USA) with ClearSeal Film (Hampton Research, USA) using the Crystal Screen, Crystal Screen 2, PEG/Ion, PEG/Ion 2 (Hampton Research, USA) and Morpheus (Molecular Dimensions, UK) screens. Three different drop ratios were aliquoted using a Mosquito nanolitre dispenser system (TTP LabTech, Melbourn, England) by mixing 75, 100 or 50 nl protein solutions with 75, 50 or 100 nl reservoir solutions, respectively. All drops were equilibrated against a 75 µl reservoir solution. A single crystal appeared in 2 d from a 1:1 ratio drop in condition No. 44 of Morpheus [the mixture of precipitants consisted of 12.5%(*w*/*v*) PEG 1000, 12.5%(*w*/*v*) PEG 3350 and 12.5%(*v*/*v*) MPD and the mixture of additives consisted of 0.02 *M* amino acids (0.2 *M* sodium L-glutamate, 0.2 *M* DL-alanine, 0.2 *M* glycine, 0.2 *M* DL-lysine–HCl, 0.2 *M* DL-serine) with buffer system 2 (0.1 *M* MOPS/HEPES–Na pH 7.5: a mixture of 26 ml 1 *M* MOPS with 24 ml 1 *M* HEPES–Na)]. Manual optimization of the crystal-growth conditions was performed using the hanging-drop vapour-diffusion method in 24-well VDX plates (Hampton Research, USA). The best crystals were grown at 293 K in drops consisting of a mixture of 1 µl protein solution and 1 µl reservoir solution; these drops were equilibrated against 200 µl reservoir solution.

A single crystal was flash-cooled directly in a liquid N_2 stream at 100 K, as the mother liquor was an adequate cryoprotectant. The S-SAD data set (referred to as PfGrx1-SAD) was collected using Cu $K\alpha$ radiation (λ = 1.54 Å) on a MAR

[1] Supporting information has been deposited in the IUCr electronic archive (Reference: RR5049).

Table 1
Summary of diffraction data and structure-refinement statistics.

Values in parentheses are for the highest resolution shell.

Data set	PfGrx1-SAD	PfGrx1-AR1	PfGrx1-AR2
PDB entry	4hjm	4kje	4kjf
Data collection			
Wavelength (Å)	1.54	0.83	0.73
Crystal-to-detector distance (mm)	100	100	82.8
Oscillation (°)	1	1	0.5
Exposure time (s)	30	6	4
No. of frames	360	360	720
Unit-cell parameters (Å, °)	$a = b = 48.09$, $c = 82.59$, $\alpha = \beta = 90$, $\gamma = 120$	$a = b = 47.95$, $c = 82.45$, $\alpha = \beta = 90$, $\gamma = 120$	$a = b = 47.97$, $c = 82.47$, $\alpha = \beta = 90$, $\gamma = 120$
Space group	$P3_221$	$P3_221$	$P3_221$
Resolution (Å)	50.0–1.55 (1.60–1.55)	50.0–1.04 (1.08–1.04)	50.0–0.95 (0.97–0.95)
Unique reflections	16595 (1399)	53655 (5261)	69290 (3474)
Multiplicity	19.0 (15.2)	21.6 (21.3)	21.0 (21.5)
Completeness (%)	97.7 (83.9)	100 (100)	100 (98.8)
$\langle I/\sigma(I)\rangle$	91.2 (13.2)	52.6 (5.7)	43.0 (6.7)
R_{merge}	0.049 (0.257)	0.058 (0.512)	0.061 (0.493)
Substructure solution and phasing			
CC_{all}/CC_{weak} (%)	35.2/21.3		
Located substructures	6		
Map contrast	0.47		
Connectivity	0.93		
Polyalanine traced	105		
Map CC (%)	47.3		
Refinement			
Resolution (Å)	50.0–1.55	24.0–1.04	24.0–0.95
Reflections in work set/test set	15732/839	50881/2722	65722/3499
R_{work}/R_{free} (%)	14.80/17.87	11.75/12.86	10.39/11.09
Model composition			
No. of residues	106	106	106
No. of waters	176	175	199
Ligand molecules			
MOPS	1	1	1
MPD	1	1	1
Stereochemistry (r.m.s.d.)			
Bond lengths (Å)	0.006	0.008	0.010
Bond angles (°)	1.093	1.384	1.475
Ramachandran plot, residues in (%)			
Most favoured regions	89.5	91.6	92.6
Additionally allowed regions	10.5	8.4	7.4
Mean B factors (Å^2)			
Protein atoms	17.6	12.5	11.6
Waters	34.5	23.6	21.4
Ligand molecules			
MOPS	15.9	8.6	8.7
MPD	34.8	37.3	36.8
MolProbity			
MolProbity score	1.19	1.24	1.46
All-atoms clashscore	4.1	4.9	8.6
Poor rotomers (%)	0	0	0
Ramachandran favoured/outliers (%)	99.0/0.0	99.0/0.0	99.0/0.0

345 image-plate detector mounted on a Rigaku MicroMax-007 rotating-anode X-ray generator operated at 40 kV and 20 mA with VariMax HR optics. A total range of 360° was covered with 1.0° oscillation and 30 s exposure per frame. The crystal-to-detector distance was set to 100 mm. X-ray diffraction data were collected to 1.55 Å resolution. Other atomic resolution data sets (referred to as PfGrx1-AR1 and PfGrx1-AR2) were collected to 1.04 and 0.95 Å resolution using two different crystals (Supplementary Fig. S2) and two different wavelengths (0.83 and 0.73 Å) on BM14, ESRF, Grenoble. All data sets were indexed, processed, and scaled using the *HKL*-2000 package (Otwinowski & Minor, 1997). Bijvoet mates were treated as equivalent reflections during scaling but were merged separately as I^+ and I^- for the S-SAD data. Crystal parameters and data-processing statistics are summarized in Table 1.

2.3. Structure determination and refinement

PfGrx1 consists of 111 amino acids (~12.4 kDa) with three methionines and three cysteines. From the crystal parameters, it was clear that there was one molecule per asymmetric unit, with a Matthews coefficient of 2.21 Å^3 Da^{-1} and a solvent content of 44%. The observed anomalous signal ($\langle\Delta F\rangle/\langle F\rangle$) was 0.02, which was higher than the expected value of 0.01 at the Cu $K\alpha$ radiation wavelength (λ = 1.54 Å) for a 111-residue protein with six S atoms (Hendrickson & Teeter, 1981; Dauter *et al.*, 2002). The mean anomalous signal-to-noise ratio [$\langle\Delta F/\sigma(\Delta F)\rangle$] was 1.47 and was significant to 2.0 Å resolution (Supplementary Table S1). Therefore, we chose the S-SAD approach to solve the phase problem. A heavy-atom position search was performed to 2.0 Å resolution with *SHELXD* (Sheldrick, 2008), and the positions of six sulfur anomalous scatterers with occupancy >0.5 were obtained (Supplementary Fig. S3). These anomalous scatterers were further used to estimate the phases with *SHELXE* (Sheldrick, 2008). The electron-density maps generated by *SHELXE* had a clear, interpretable electron density, and 105 out of 111 polyalanine residues could be built in three chains (Fig. 1*a*). Furthermore, automatic model building was carried out with *ARP*/*wARP* (Langer *et al.*, 2008) using the amino-acid sequence of PfGrx1, a polyalanine model, and the phases from *SHELXE*. The unit-cell parameters of the atomic resolution data sets (PfGrx1-AR1 and PfGrx1-AR2) were isomorphous to those for the PfGrx1-SAD data set. Therefore, atomic resolution structures were determined by 20 cycles of rigid-body refinement using *REFMAC*5 (Murshudov *et al.*, 2011) from the *CCP*4 suite (Winn *et al.*, 2011) with the PfGrx1-SAD structure as a model Subsequently, a few runs of ten cycles of restrained refinement were carried out using *REFMAC*5. After each step of refinement, the models were inspected and manually adjusted to correspond to computed $2F_o - F_c$ and $F_o - F_c$

electron-density maps using *Coot* (Emsley & Cowtan, 2004). During the progress of the refinement, 3-(*N*-morpholino)-propanesulfonic acid (MOPS) and 2-methyl-2,4-pentanediol (MPD) solvent molecules and water molecules were manually added and included in the refinement based on positive peaks in difference Fourier maps. The final round of refinement was carried out using *phenix.refine* (Afonine *et al.*, 2012). The occupancies of alternate conformations of protein residues and water molecules were also refined. The quality of the atomic model was assessed with *PROCHECK* (Laskowski *et al.*, 1993) and *MolProbity* (Chen *et al.*, 2010). The figures were generated using *Chimera* (Pettersen *et al.*, 2004) and *PyMOL* (http://www.pymol.org). Atomic coordinates and structure factors for the PfGrx1-SAD, PfGrx1-AR1 and PfGrx1-AR2 data sets have been deposited in the Protein Data Bank, Research Collaboratory for Structural Bioinformatics, Rutgers University, New Brunswick, New Jersey, USA (http://www.rcsb.org/) with accession codes 4hjm, 4kje and 4kjf, respectively. The Friedel pairs for the S-SAD data were also included in the deposited structure factors.

3. Results and discussion

3.1. Model quality and overall description of PfGrx1

PfGrx1 has the typical glutaredoxin/thioredoxin fold with a core four-stranded β-sheet (strands β1 and β2 are parallel, and strands β3 and β4 are antiparallel) flanked by five α-helices (helices α1–α5; Fig. 1*b*). Very clear electron density was observed for all regions of the protein model except for the five N-terminal residues. *SHELXD* located an additional sulfur anomalous scatterer situated at the $^{\gamma}$Glu of the GSH-binding site. Based on electron-density maps, this site was identified as the S atom of a bound buffer solvent molecule: 3(*N*-morpholino)propanesulfonic acid (MOPS; Fig. 1*c* and Supplementary Fig. S4*a*). Additionally, a molecule of the crystallization precipitant 2-methyl-2,4-pentanediol (MPD) was found in the PfGrx1 structures (Fig. 1*d* and Supplementary Fig. S4*b*). The final refinement statistics and model parameters are summarized in Table 1. At atomic resolution, it is possible to refine alternate conformations of protein residues, bound ligands and water molecules (Dauter *et al.*, 1995; Sekar *et al.*, 2006; Liebschner *et al.*, 2013). In all three PfGrx1 structures, 13–23 residues were modelled with alternate conformations, and most of these residues were polar/charged and solvent-exposed (Supplementary Table S2). Three buried residues (Ile21, Met48 and Arg78) were also modelled with alternate conformations. The orientations of the side chains were similar for most of the alternate conformations in all structures. The refined occupancy difference was less than 0.2 for the majority of the residues in all three structures. The r.m.s.d.s between the C$^{\alpha}$ atoms of the PfGrx1-SAD, PfGrx1-AR1 and PfGrx1-AR2 structures are insignificant (<0.07 Å). An analysis of Ramachandran plots calculated by *MolProbity* (Chen *et al.*, 2010) showed that more than 99% of residues were in favoured regions, and the remainder (less than 1%) were in allowed regions.

3.2. The active-site thiols and radiation-induced changes

The active-site cysteine pair containing the motif 29-CPYC-32 is located in a loop connecting the β1 strand to the α2 helix (Fig. 1*b*). The dithiol CPYC motif is identical to the active-site motif in ScGrx1 (PDB entries 3c1r and 3c1s; Yu *et al.*, 2008; Table 2), ScGrx2 (PDB entries 3ctf, 3ctg and 3d4m; Discola *et al.*, 2009; Li, Yu *et al.*, 2010) and SmTGR (PDB entries 2v6o, 2x99, 2x8c and 2x8g; Angelucci *et al.*, 2008, 2010). It is also very similar to CPFC motifs in EvGrx (PDB entries 2hze and 2hef; Bacik & Hazes, 2007), SsGrx1 (PDB entry 1kte; Katti *et al.*, 1995) and HsGrx2 (PDB entries 2fls and 2ht9; Structural Genomics Consortium, unpublished work; Johansson *et al.*,

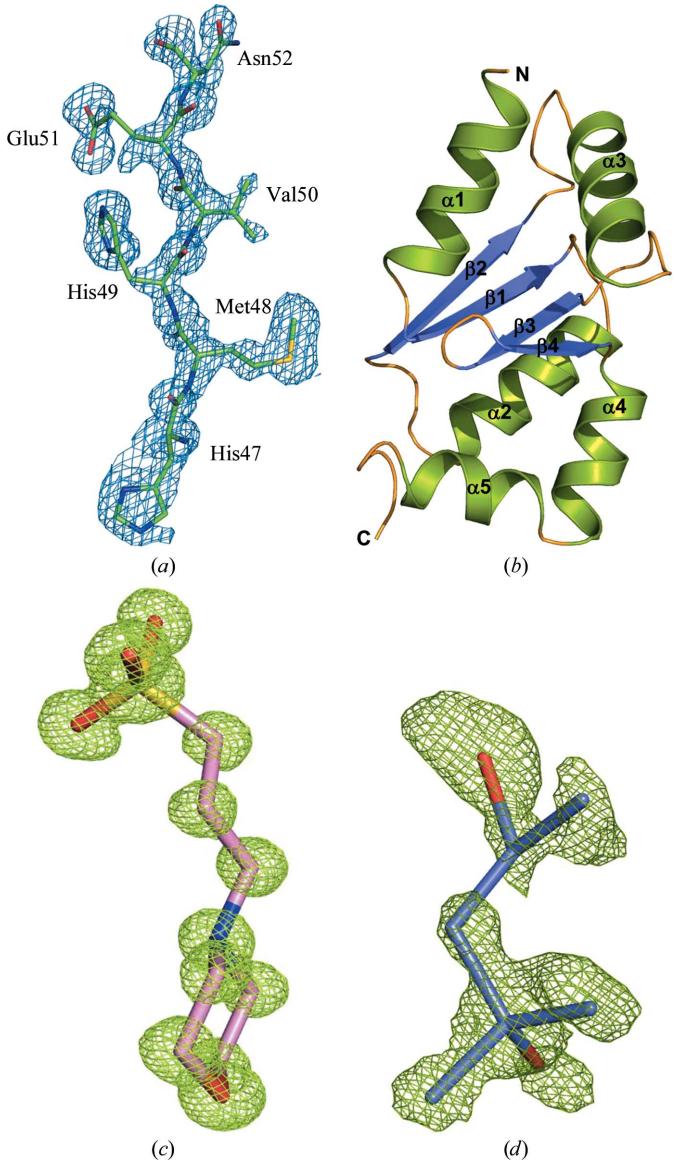

Figure 1
(*a*) A portion of the electron-density map from *SHELXE* (after phasing and solvent flattening) along with the final PfGrx1 structure. The map is contoured at 3σ. (*b*) Cartoon diagram of the PfGrx1 structure. Secondary structural elements are labelled along with the protein termini. (*c*) OMIT difference electron-density map contoured at the 5σ level showing MOPS bound to the PfGrx1 structure. (*d*) OMIT difference electron-density map contoured at the 3σ level showing bound MPD.

2007). The continuous electron density between the S atoms of Cys29 and Cys32 shows an oxidized disulfide bond in PfGrx1-SAD and PfGrx-AR1 (Figs. 2*a* and 2*b*). The refined disulfide-bond lengths in PfGrx1-SAD and PfGrx1-AR1 are 2.05 and 2.10 Å, respectively; similar disulfide distances (2.06–2.08 Å) were observed in oxidized Grx structures (Katti *et al.*, 1995; Yu *et al.*, 2008; Bacik & Hazes, 2007; Discola *et al.*, 2009; Li, Yu *et al.*, 201) as well as in a survey of S—S distances [(2.04 (16) Å] in protein structures (Morris *et al.*, 1992). The refined disulfide distance in PfGrx1-AR2 is 2.23 Å. Disulfide bond breakage can occur when using high-energy X-ray beams for diffraction data collection (Ravelli & McSweeney, 2000; Burmeister, 2000; Liebschner *et al.*, 2013): S—S bond lengths first elongate and then break under the influence of absorbed X-rays. We therefore inspected difference electron-density maps around the disulfide bridge in the PfGrx1 structures to identify the likelihood of S—S bond breakage or alternate positions of S^{γ} atoms that are not connected to their partners. In PfGrx1-AR2, a strong negative density peak (8–10σ level) was observed at the Cys29–Cys32 bridge, whereas in PfGrx1-AR1 a negative peak (<6σ level) was only observed for the S^{γ} atom of Cys29. In PfGrx1-AR2, a positive peak (6–8σ level) was observed near Cys29 so that an alternate position of the S^{γ} atom could be located. The positive peak near Cys29 in PfGrx1-AR1 is significantly weaker (<4σ level), and no alternate position could be located. The refined occupancies in the *A* and *B* conformations are 0.65 and 0.35, respectively. The major conformation of Cys29 was still connected to its partner Cys32. The normalized χ^2 values indicate that the PfGrx1-AR2 data set (χ^2 = 1.131) suffered more radiation damage than the

Table 2
Comparison of PfGrx1 with Grxs and Grx-like domains.

No.	PDB code	Source† and name	No. of residues	No. of superposed C^{α} atoms	R.m.s.d. (Å)	Identity (%)	Active-site motif	Reference
1	3c1r	ScGrx1	110	104	1.6	37	CPYC	Yu *et al.* (2008)
2	1kte	SsGrx1	105	103	1.8	37	CPFC	Katti *et al.* (1995)
3	3ctg	ScGrx2	108	104	1.6	31	CPYC	Li, Yu *et al.* (2010)
4	3fz9	PtGrxS12	106	102	1.5	31	CSYS	Couturier *et al.* (2009)
5	2fls	HsGrx2	101	100	1.3	29	CSYC	
6	3rhb	AtGrxC5	100	99	1.3	28	CSYC	Couturier *et al.* (2011)
7	2e7p	PtGrxC1	101	101	1.4	28	CGYC	Rouhier *et al.* (2007)
8	3qmx	SyGrxA	99	82	1.5	28	CPFC	Kim *et al.* (2012)
9	3l4n	ScGrx6	113	104	2.0	26	CSYS	Luo *et al.* (2010)
10	2hze	EvGrx	110	103	1.8	25	CPFC	Bacik & Hazes (2007)
11	3ipz	AtGrxcp	109	99	1.9	23	CGFS	Li, Cheng *et al.* (2010)
12	1aaz	EpGrx	87	74	2.2	23	CVYC	Eklund *et al.* (1992)
13	2wul	HsGrx5	109	99	1.7	22	CGFS	Johansson *et al.* (2011)
14	3gx8	ScGrx5	111	102	1.6	21	CGFS	
15	3msz	FtGrx1	87	81	1.8	21	CPYC	
16	2x99	SmTGR	587	99	1.6	20	CPYC	Angelucci *et al.* (2010)
17	2wci	EcGrx4	113	99	2.0	20	CGFS	Iwema *et al.* (2009)
18	2yan	HsTXLN2	105	97	2.1	16	CGFS	
19	3zyw	HsGrx3D1	111	99	2.3	16	CGFS	

† At, *Arabidopsis thaliana*; Ec, *Escherichia coli*; Ev, *Ectromelia virus*; Hs, *Homo sapiens*; Pt, *Populus tremula* × *P. tremuloides*; Ss, *Sus scrofa*; Sc, *Saccharomyces cerevisiae*; Sm, *Schistosoma mansoni*; Sy, *Synechocystis* sp.

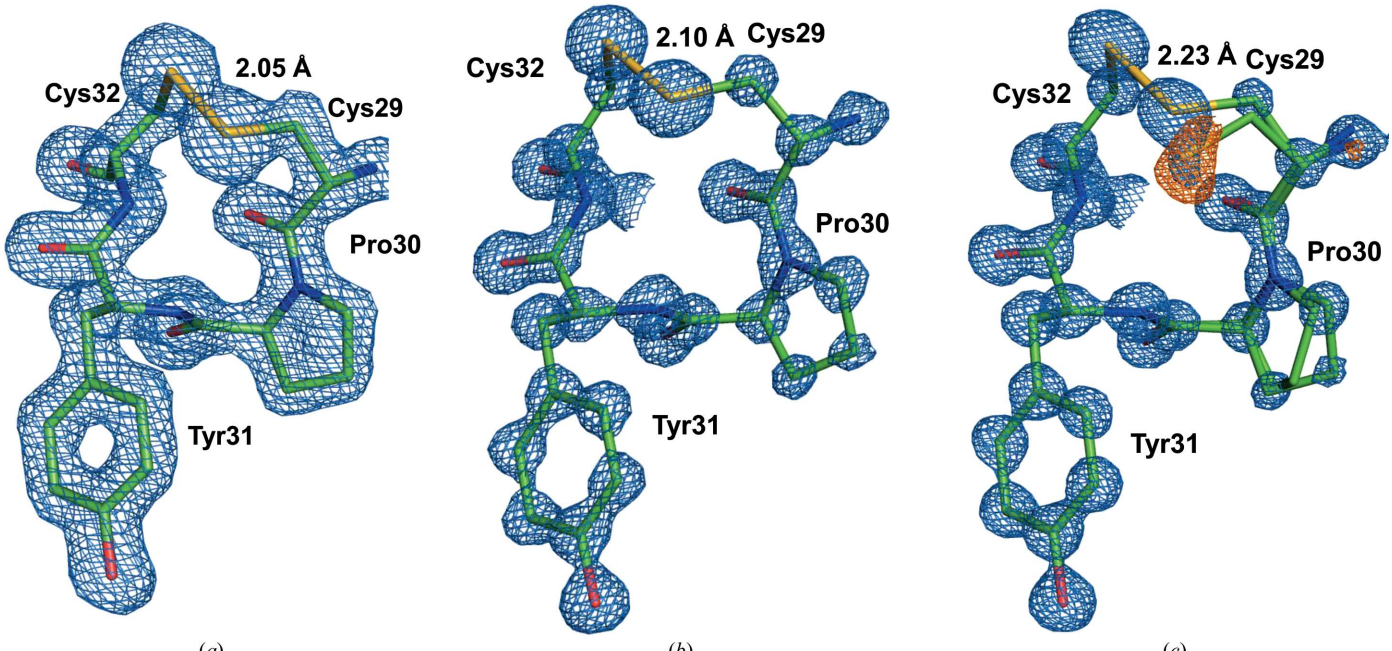

(*a*) (*b*) (*c*)

Figure 2
The active-site CPYC motif in the (*a*) PfGrx1-SAD, (*b*) PfGrx1-AR1 and (*c*) PfGrx1-AR2 structures. The final $2F_o - F_c$ map is contoured at 1.5σ for PfGrx1-SAD and is contoured at 3σ for both PfGrx1-AR1 and PfGrx1-AR2. The difference Fourier ($F_o - F_c$) map at the 3σ level (orange) shows an alternate position of Cys29 in PfGrx1-AR2.

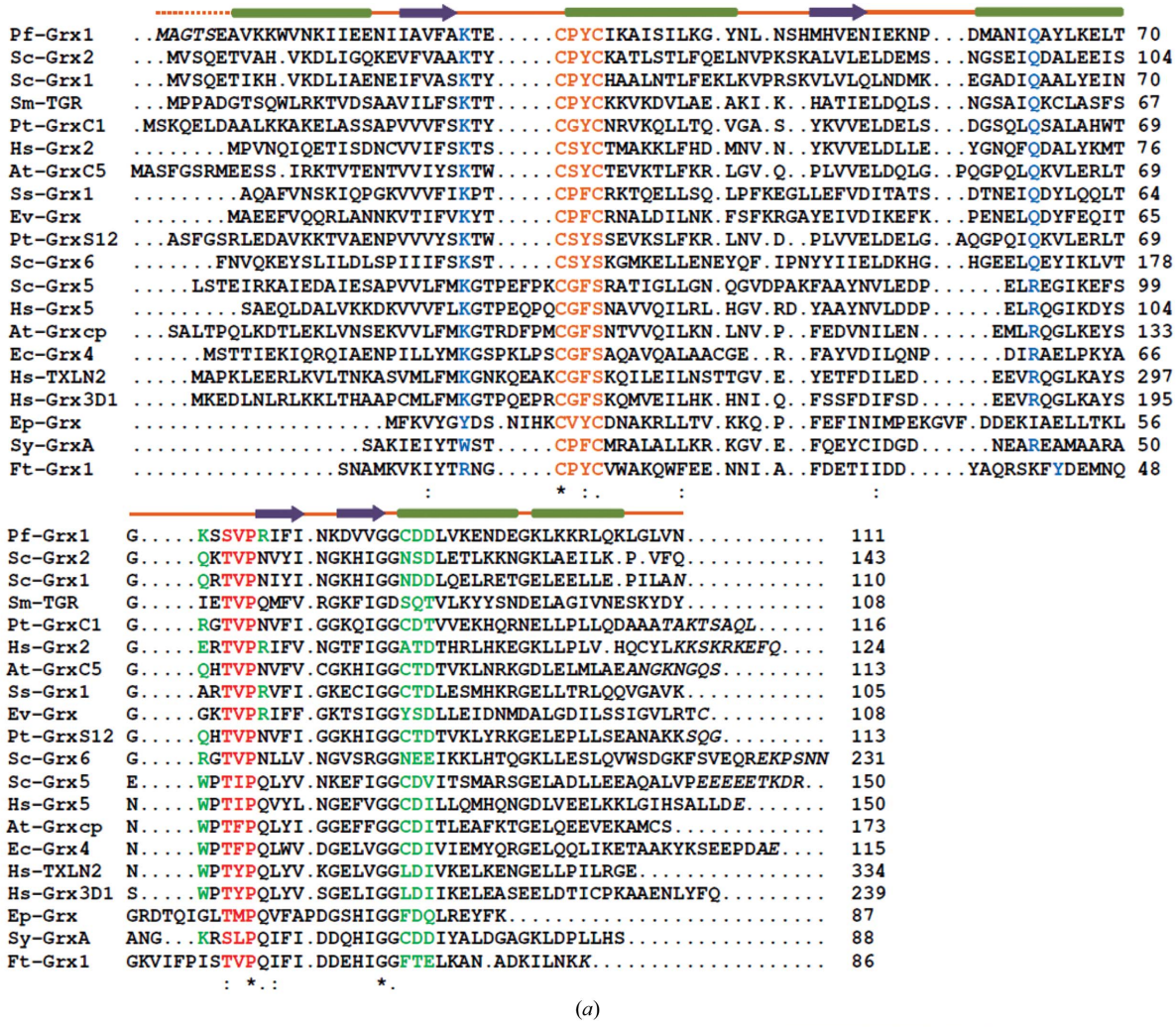

Figure 3
(*a*) Structure-based sequence alignment of Grxs (refer to Table 2 for PDB codes and organism information). Identical, conserved and semi-conserved residues are marked with asterisks, colons and dots, respectively. The active-site residues (C*XX*C for dithiol Grx and C*XX*S for monothiol Grx) and atoms involved in interactions with Gly, Cys and $^{\gamma}$Glu of GSH are highlighted in blue, orange and red, and green, respectively. (*b*) A superposition of C^{α} atoms of Grxs is shown. Apart from insertion regions, the largest deviations are observed in the α1, α3 and α5 helices. Identical, conserved, semi-conserved and weakly conserved residues are rendered in red, pink, grey and blue, respectively. (*c*) Comparison of GSH-binding site motifs in Grxs. Positions of conserved C*XX*C/C*XX*S (cyan), TVP (yellow), CDD (green) motifs and Lys26 (orange) and Gln/Arg63 (blue) residues are highlighted. The conserved Gly-Gly doublet is also marked. Bound GSH molecules (pink) are shown as ball-and-stick models.

PfGrx1-AR1 data set (χ^2 = 0.839). The deposited radiation dose was calculated using *RADDOSE* (Zeldin *et al.*, 2013). The average and maximum doses deposited were 6.9 and 67.9 kGy, respectively, for the PfGrx1-AR1 crystals and 7.9 and 78.6 kGy, respectively, for the PfGrx1-AR2 crystals. Therefore, radiation damage may be limited. The average *B* factor of the active-site CPYC motif in the PfGrx1 structures (14.4, 8.4 and 8.5 Å^2 for PfGrx1-SAD, PfGrx1-AR1 and PfGrx1-AR2, respectively) is lower than the overall *B* values (Table 1), which are similar to those of other dithiol Grxs (Rouhier *et al.*, 2007; Yu *et al.*, 2008; Discola *et al.*, 2009; Li, Yu *et al.*, 2010).

3.3. Structural comparison of PfGrx1 with other Grxs/Grx-like domains

The sequence identity between Grxs and Grx-like domains is in the range 16–37% and few residues (<15) are conserved among them (Fig. 3*a* and Table 2). The superposition of 74–104 C$^\alpha$ atoms of the PfGrx1 structure with monothiol/dithiol, oxidized/reduced and GSH-bound/unbound forms of Grx structures from different organisms shows an r.m.s.d. range of 1.3–2.3 Å (Fig. 3*b* and Table 2), suggesting that the overall folding of PfGrx1 is similar to that of other Grxs and Grx-like domains. Superposition of Grxs and Grx-like domains shows very good agreement for the core β-strands and the active-site motif containing the α2 helix and the α4 helix (Fig. 3*b*). Apart from the insertion loops, the maximum displacement was observed in the α1, α3 and α5 helices. Most conserved residues are present around the active-site regions of these enzymes (Fig. 3*b*). The GSH-binding motifs (C*XX*C or C*XX*S, TVP and CDD) are structurally conserved in oxidized/reduced and GSH-bound/unbound forms of both the monothiol and dithiol Grxs except for the Gly-binding residue at position 63 (Fig. 3*c*). In most Grxs, a conserved hydrophobic residue followed by a Gly-Gly doublet precedes the CDD motif. The Gly-Gly doublet provides room for two conserved water molecules (Wc1 and Wc2) which interact with the $^\gamma$Glu of GSH. Bound GSH molecules adopt extended conformations apart from in FtGrx (PDB entry 3msz; Fig. 3*c*). In all Grxs, highly positively charged surfaces were observed in the GSH chelating regions; however, distinct surfaces were observed between the Gly- and $^\gamma$Glu-binding sites (Fig. 4). The basic charge congregations are owing to the conserved residues Lys and Gln/Arg at

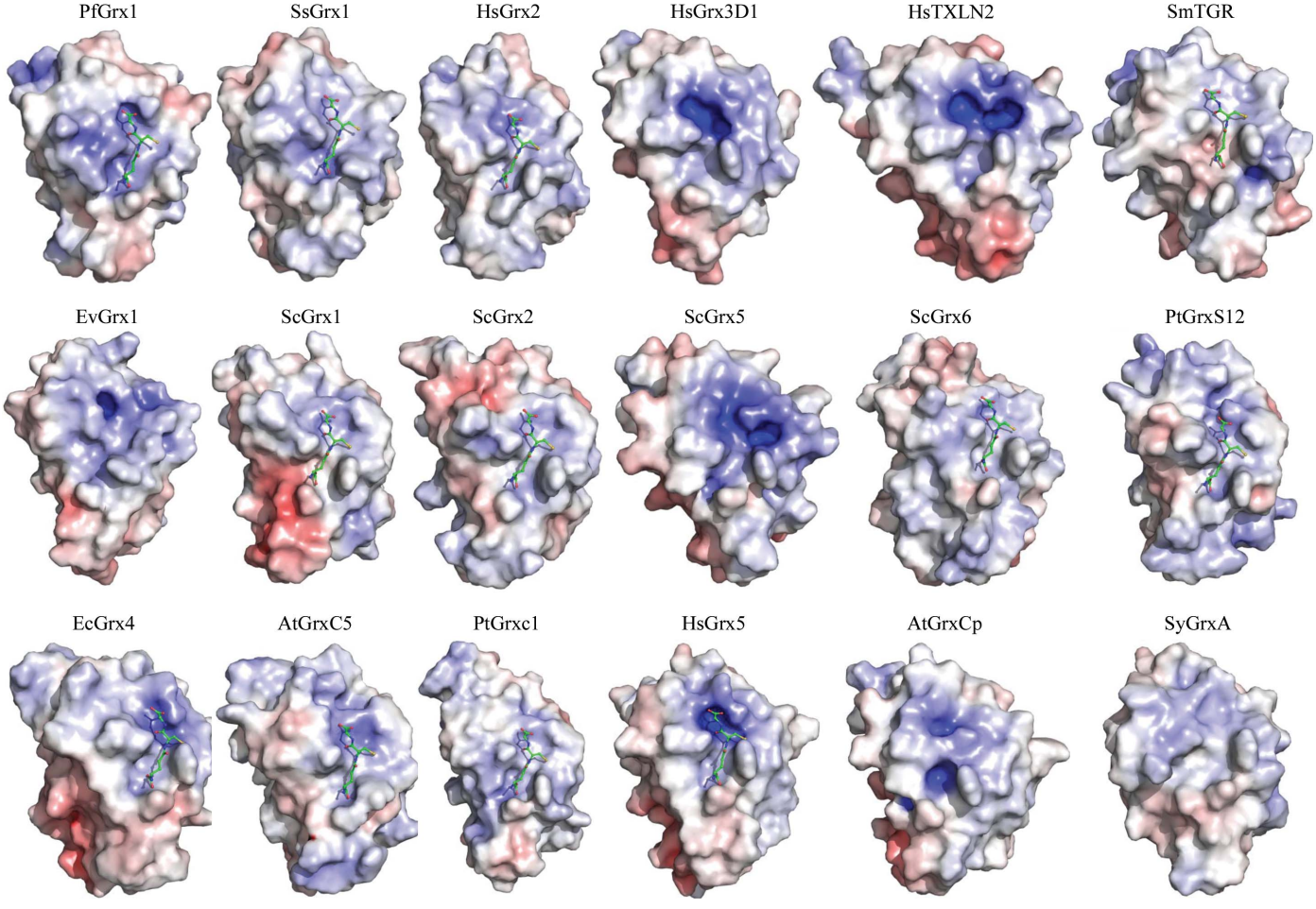

Figure 4
Comparison of electrostatic potential on the molecular surface of Grxs. Bound GSH is shown as a ball-and-stick model. GSH is shown in PfGrx1 and SsGrx1 based on overlay with HsGrx2. The electrostatic surface is displayed as a colour gradient in red (electronegative, $\leq -10\ kT\ e^{-1}$) and blue (electropositive, $\geq 10\ kT\ e^{-1}$).

positions 26 (based on the PfGrx1 residue numbering) and 63, respectively. The distinct potential distribution in the $^{\gamma}$Glu-binding region is a consequence of fewer conserved residues in the CDD motif as well as at positions 72 (Lys/Arg/Gln/Trp) and 77 (Arg/Gln/Asn) (Fig. 3*a*).

3.4. GSH-binding site in PfGrx1

The solvent-exposed GSH-binding channel in PfGrx1 is filled with several water molecules, and the $^{\gamma}$Glu portion of the GSH-binding pocket is occupied by MOPS (Figs. 1*c* and 5*a*, and Supplementary Figs. S3 and S4*a*). Bound MOPS interacts with the CDD and TVP motifs. The *B* factor of the bound MOPS molecule is lower than that of the protein atoms in all three PfGrx1 structures (Table 1). Our co-crystallization and cryo-soaking attempts failed to provide crystals of the PfGrx1–GSH complex. This may be owing to a higher binding affinity of PfGrx1 for buffer molecules (Fig. 5*a*). Therefore, we modelled the GSH molecule into the PfGrx1 active site by superimposing GSH-bound HsGrx2 (PDB entry 2fls; Structural Genomics Consortium, unpublished work) onto PfGrx1 (Fig. 5*b*). The backbone carboxyl O and amide N atoms of Cys and $^{\gamma}$Gly in GSH invariantly interact with the backbone N and O atoms of the conserved TVP (Thr-Val-Pro) and CDD (Cys-Asp-Asp) motifs. In the present atomic resolution PfGrx1 structures, six GSH binding pocket residues (Lys26, Cys29, Pro30, Lys72, Arg77 and Asp90) adopt alternate conformations. In PfGrx1, polygonal water structures such as tetragons and pentagons were observed (Fig. 5*a* and Supplementary Fig. S4a). Hydrogen-bonding interactions between Lys26 and Gln63 are absent in PfGrx1 when compared with other GSH-bound and free Grxs (ScGrx1 and ScGrx2; PDB entries 3c1r, 3c1s, 3ctf, 3ctg and 3d4m; Yu *et al.*, 2008; Li, Yu *et al.*, 2010; Discola *et al.*, 2009).

3.5. Conserved water molecules and unique features of PfGrx1

Three conserved water molecules (Wc1, Wc2 and Wc3) are observed for most Grxs (Figs. 3*c* and 5*c*). Wc1 and Wc2 are located at the GSH-binding site and are involved in hydrogen-bonding interactions between the GSH molecule and the TVP and CDD motifs. The other conserved water molecule Wc3 is

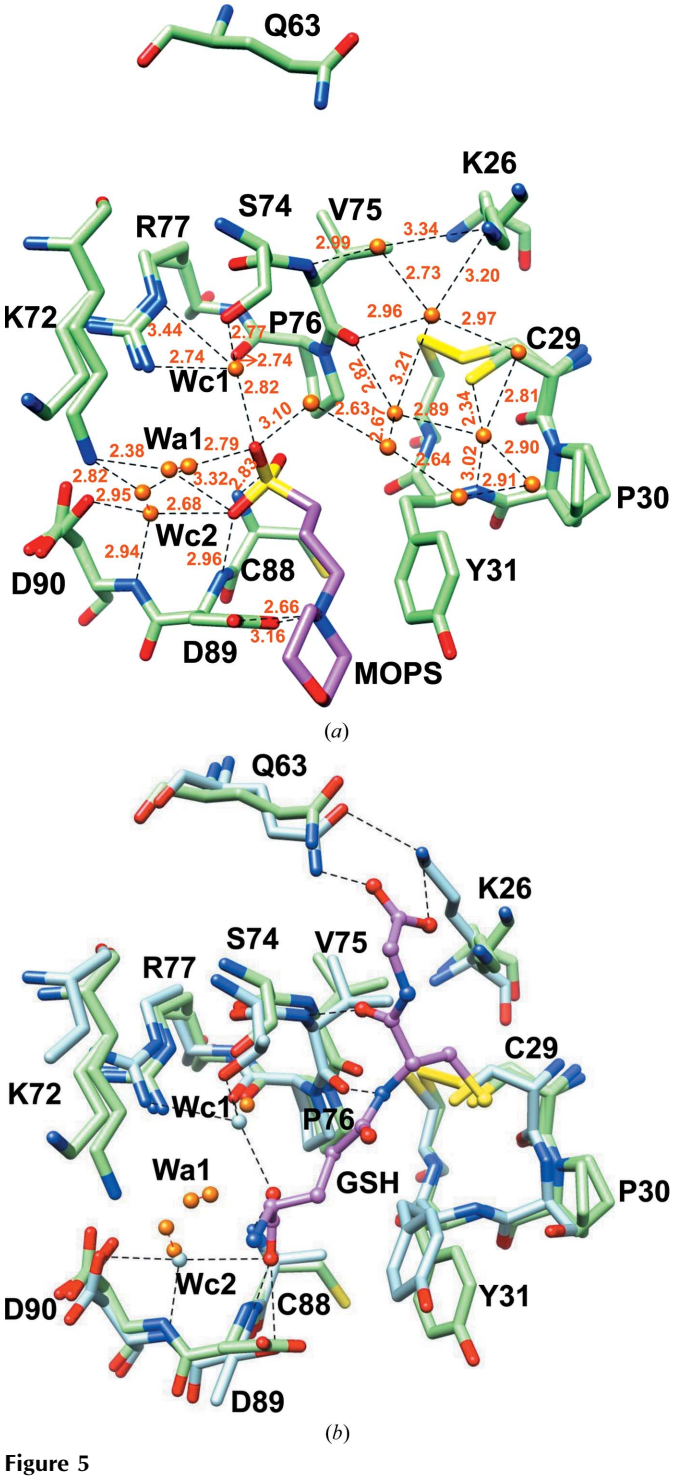

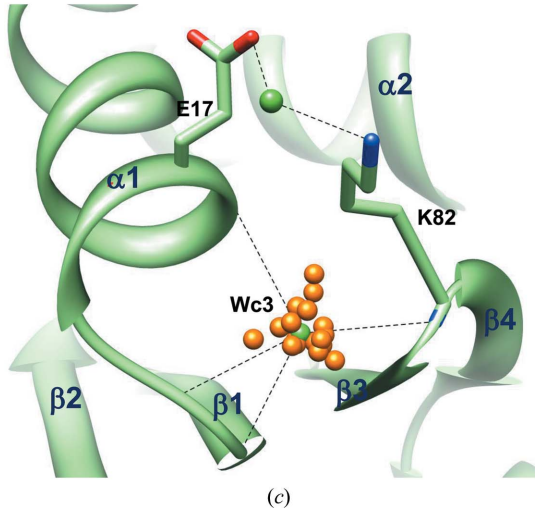

Figure 5
(*a*) The GSH-binding site in PfGrx1. Bound MOPS (pink) and water molecules (orange spheres) are shown. Atom interactions are shown as dashed lines. (*b*) Superposition of the active sites of PfGrx1 (green) and glutathionylated HsGrx2 (blue). (*c*) A water molecule that is structurally conserved in Grxs is shown. An additional water-mediated salt bride in PfGrx1 is also shown.

located at the position of the α1 helix, the β1 strand, and the loop between the β3 and β4 strands. In PfGrx1, Glu28 precedes the active-site residues, and the corresponding position in other Grxs is populated by polar Ser/Thr/Asn, aromatic Tyr/Trp, or Gly residues. Similarly, Glu51 is located between the α1 helix and the β2 strand, and the corresponding position in other Grxs has a conserved hydrophobic residue Val/Leu/Ile or aromatic residue Phe/Tyr (Fig. 3*a*). A water-mediated salt bridge between the α1 helix and the loop between the β3 and β4 strands is found in PfGrx1, and this interaction is absent in other Grxs (Fig. 5*c*). Unique salt bridges between the α1 and α3 helices and the β4 strand and the α4 and α5 helices were found only in PfGrx1, PtGrxS12 and SsGrx1 (Supplementary Fig. S5).

4. Conclusions

In this work, we have determined the atomic structure of the dithiol Grx PfGrx1 and compared it in depth with those of other Grxs from different organisms. Our results indicate that monothiol (C*XX*S) and dithiol (C*XX*C) Grxs differ significantly in their helix-capping hydrogen bonds (Supplementary Figs. S6, S7 and S8). Both monothiol and dithiol Grxs contain three conserved water molecules, of which two are located in the GSH-binding site while the third is located between β-strands and the α1 helix. The dithiol-containing redox proteins thioredoxin (Trx), glutaredoxin (Grx) and plasmoredoxin (Plrx), with the latter being exclusively found in *Plasmodium* species, play central roles in maintaining redox homeostasis in malarial parasites (Sturm *et al.*, 2009). The PfGrx1 structure presented here in complex with MOPS and MPD provides novel insights concerning interacting surfaces whose roles in *in vivo* interactions with parasite biomolecules remain to be explored in further detail.

The X-ray facility at ICGEB was funded by the Wellcome Trust. This work was generously supported with grants from the Department of Biotechnology (DBT), Government of India to TT, AS and MY, and with the Deutsche Forschungsgemeinschaft (BE 1540/18-1 to KB and SR).

References

Afonine, P. V., Grosse-Kunstleve, R. W., Echols, N., Headd, J. J., Moriarty, N. W., Mustyakimov, M., Terwilliger, T. C., Urzhumtsev, A., Zwart, P. H. & Adams, P. D. (2012). *Acta Cryst.* D**68**, 352–367.
Angelucci, F., Dimastrogiovanni, D., Boumis, G., Brunori, M., Miele, A. E., Saccoccia, F. & Bellelli, A. (2010). *J. Biol. Chem.* **285**, 32557–32567.
Angelucci, F., Miele, A. E., Boumis, G., Dimastrogiavanni, D., Brunori, M. & Belleli, A. (2008). *Proteins*, **72**, 936–945.
Axelsson, K. & Mannervik, B. (1980). *Biochim. Biophys. Acta*, **613**, 324–336.
Bacik, J. P. & Hazes, B. (2007). *J. Mol. Biol.* **365**, 1545–1558.
Balmer, Y., Koller, A., del Val, G., Manieri, W., Schürmann, P. & Buchanan, B. B. (2003). *Proc. Natl Acad. Sci. USA*, **100**, 370–375.
Berndt, C., Lillig, C. H. & Holmgren, A. (2008). *Biochim. Biophys. Acta*, **1783**, 641–650.
Burmeister, W. P. (2000). *Acta Cryst.* D**56**, 328–341.
Chen, V. B., Arendall, W. B., Headd, J. J., Keedy, D. A., Immormino, R. M., Kapral, G. J., Murray, L. W., Richardson, J. S. & Richardson, D. C. (2010). *Acta Cryst.* D**66**, 12–21.
Chrestensen, C. A., Starke, D. W. & Mieyal, J. J. (2000). *J. Biol. Chem.* **275**, 26556–26565.
Couturier, J., Koh, C. S., Zaffagnini, M., Winger, A. M., Gualberto, J. M., Corbier, C., Decottignies, P., Jacquot, J.-P., Lemaire, S. D., Didierjean, C. & Rouhier, N. (2009). *J. Biol. Chem.* **284**, 9299–9310.
Couturier, J., Ströher, E., Albetel, A. N., Roret, T., Muthuramalingam, M., Tarrago, L., Seidel, T., Tsan, P., Jacquot, J.-P., Johnson, M. K., Dietz, K. J., Didierjean, C. & Rouhier, N. (2011). *J. Biol. Chem.* **286**, 27515–27527.
Dauter, Z., Dauter, M. & Dodson, E. J. (2002). *Acta Cryst.* D**58**, 494–506.
Dauter, Z., Lamzin, V. S. & Wilson, K. S. (1995). *Curr. Opin. Struct. Biol.* **5**, 784–790.
Discola, K. F., de Oliveira, M. A., Rosa Cussiol, J. R., Monteiro, G., Bárcena, J. A., Porras, P., Padilla, C. A., Guimarães, B. G. & Netto, L. E. (2009). *J. Mol. Biol.* **385**, 889–901.
Djuika, C. F., Fiedler, S., Schnölzer, M., Sanchez, C., Lanzer, M. & Deponte, M. (2013). *Biochim. Biophys. Acta*, **1830**, 4073–4090.
Eklund, H., Ingelman, M., Söderberg, B. O., Uhlin, T., Nordlund, P., Nikkola, M., Sonnerstam, U., Joelson, T. & Petratos, K. (1992). *J. Mol. Biol.* **228**, 596–618.
Emsley, P. & Cowtan, K. (2004). *Acta Cryst.* D**60**, 2126–2132.
Feng, Y., Zhong, N., Rouhier, N., Hase, T., Kusunoki, M., Jacquot, J.-P., Jin, C. & Xia, B. (2006). *Biochemistry*, **45**, 7998–8008.
Fernandes, A. P. & Holmgren, A. (2004). *Antioxid. Redox Signal.* **6**, 63–74.
Gallogly, M. M., Starke, D. W. & Mieyal, J. J. (2009). *Antioxid. Redox Signal.* **11**, 1059–1081.
Gonzalez Porqué, P., Baldesten, A. & Reichard, P. (1970). *J. Biol. Chem.* **245**, 2371–2374.
Hendrickson, W. A. & Teeter, M. M. (1981). *Nature (London)*, **290**, 107–113.
Hoff, K. G., Culler, S. J., Nguyen, P. Q., McGuire, R. M., Silberg, J. J. & Smolke, C. D. (2009). *Chem. Biol.* **16**, 1299–1308.
Holmgren, A. (1976). *Proc. Natl Acad. Sci. USA*, **73**, 2275–2279.
Holmgren, A. (1979). *J. Biol. Chem.* **254**, 3672–3678.
Holmgren, A. (2000). *Antioxid. Redox Signal.* **2**, 811–820.
Holmgren, A., Johansson, C., Berndt, C., Lönn, M. E., Hudemann, C. & Lillig, C. H. (2005). *Biochem. Soc. Trans.* **33**, 1375–1377.
Iwema, T., Picciocchi, A., Traore, D. A. K., Ferrer, J.-L., Chauvat, F. & Jacquamet, L. (2009). *Biochemistry*, **48**, 6041–6043.
Johansson, C., Kavanagh, K. L., Gileadi, O. & Oppermann, U. (2007). *J. Biol. Chem.* **282**, 3077–3082.
Johansson, C., Roos, A. K., Montano, S. J., Sengupta, R., Filippakopoulos, P., Guo, K., von Delft, F., Holmgren, A., Oppermann, U. & Kavanagh, K. L. (2011). *Biochem. J.* **433**, 303–311.
Katti, S. K., Robbins, A. H., Yang, Y. & Wells, W. W. (1995). *Protein Sci.* **4**, 1998–2005.
Kehr, S., Sturm, N., Rahlfs, S., Przyborski, J. M. & Becker, K. (2010). *PLoS Pathog.* **6**, e1001242.
Kim, S. G., Chung, J.-S., Sutton, R. B., Lee, J.-S., López-Maury, L., Lee, S. Y., Florencio, F. J., Lin, T., Zabet-Moghaddam, M., Wood, M. J., Nayak, K., Madem, V., Tripathy, J. N., Kim, S.-K. & Knaff, D. B. (2012). *Biochim. Biophys. Acta*, **1824**, 392–403.
Langer, G., Cohen, S. X., Lamzin, V. S. & Perrakis, A. (2008). *Nature Protoc.* **3**, 1171–1179.
Laskowski, R. A., MacArthur, M. W., Moss, D. S. & Thornton, J. M. (1993). *J. Appl. Cryst.* **26**, 283–291.
Lemaire, S. D., Guillon, B., Le Maréchal, P., Keryer, E., Miginiac-Maslow, M. & Decottignies, P. (2004). *Proc. Natl Acad. Sci. USA*, **101**, 7475–7480.
Li, L., Cheng, N., Hirschi, K. D. & Wang, X. (2010). *Acta Cryst.* D**66**, 725–732.

Li, W.-F., Yu, J., Ma, X.-X., Teng, Y.-B., Luo, M., Tang, Y.-J. & Zhou, C.-Z. (2010). *Biochem. Biophys. Acta*, **1804**, 1542–1547.
Liebschner, D., Dauter, M., Brzuszkiewicz, A. & Dauter, Z. (2013). *Acta Cryst.* D**69**, 1447–1462.
Lill, R., Dutkiewicz, R., Elsässer, H. P., Hausmann, A., Netz, D. J., Pierik, A. J., Stehling, O., Urzica, E. & Mühlenhoff, U. (2006). *Biochim. Biophys. Acta*, **1763**, 652–667.
Lillig, C. H., Berndt, C. & Holmgren, A. (2008). *Biochim. Biophys. Acta*, **1780**, 1304–1317.
Lillig, C. H., Berndt, C., Vergnolle, O., Lönn, M. E., Hudemann, C., Bill, E. & Holmgren, A. (2005). *Proc. Natl Acad. Sci. USA*, **102**, 8168–8173.
Lindahl, M. & Florencio, F. J. (2003). *Proc. Natl Acad. Sci. USA*, **100**, 16107–16112.
Luo, M., Jiang, Y.-L., Ma, X.-X., Tang, Y.-J., He, Y.-X., Yu, J., Zhang, R.-G., Chen, Y. & Zhou, C.-Z. (2010). *J. Mol. Biol.* **398**, 614–622.
Matthews, J. R., Wakasugi, N., Virelizier, J. L., Yodoi, J. & Hay, R. T. (1992). *Nucleic Acids Res.* **20**, 3821–3830.
Morris, A. L., MacArthur, M. W., Hutchinson, E. G. & Thornton, J. M. (1992). *Proteins*, **12**, 345–364.
Motohashi, K., Kondoh, A., Stumpp, M. T. & Hisabori, T. (2001). *Proc. Natl Acad. Sci. USA*, **98**, 11224–11229.
Mühlenhoff, U., Molik, S., Godoy, J. R., Uzarska, M. A., Richter, N., Seubert, A., Zhang, Y., Stubbe, J., Pierrel, F., Herrero, E., Lillig, C. H. & Lill, R. (2010). *Cell Metab.* **12**, 373–385.
Murshudov, G. N., Skubák, P., Lebedev, A. A., Pannu, N. S., Steiner, R. A., Nicholls, R. A., Winn, M. D., Long, F. & Vagin, A. A. (2011). *Acta Cryst.* D**67**, 355–367.
Otwinowski, Z. & Minor, W. (1997). *Methods Enzymol.* **276**, 307–326.
Pettersen, E. F., Goddard, T. D., Huang, C. C., Couch, G. S., Greenblatt, D. M., Meng, E. C. & Ferrin, T. E. (2004). *J. Comput. Chem.* **25**, 1605–1612.
Pineda-Molina, E., Klatt, P., Vázquez, J., Marina, A., García de Lacoba, M., Pérez-Sala, D. & Lamas, S. (2001). *Biochemistry*, **40**, 14134–14142.
Rahlfs, S., Fischer, M. & Becker, K. (2001). *J. Biol. Chem.* **276**, 37133–37140.
Ravelli, R. B. G. & McSweeney, S. M. (2000). *Structure*, **8**, 315–328.
Rouhier, N., Unno, H., Bandyopadhyay, S., Masip, L., Kim, S.-K., Hirasawa, M., Gualberto, J. M., Lattard, V., Kusunoki, M., Knaff, D. B., Georgiou, G., Hase, T., Johnson, M. K. & Jacquot, J.-P. (2007). *Proc. Natl Acad. Sci. USA*, **104**, 7379–7384.
Rouhier, N., Villarejo, A., Srivastava, M., Gelhaye, E., Keech, O., Droux, M., Finkemeier, I., Samuelsson, G., Dietz, K. J., Jacquot, J.-P. & Wingsle, G. (2005). *Antioxid. Redox Signal.* **7**, 919–929.
Sekar, K., Yogavel, M., Gayathri, D., Velmurugan, D., Krishna, R., Poi, M.-J., Dauter, Z., Dauter, M. & Tsai, M.-D. (2006). *Acta Cryst.* F**62**, 1–5.
Sheldrick, G. M. (2008). *Acta Cryst.* A**64**, 112–122.
Shelton, M. D., Chock, P. B. & Mieyal, J. J. (2005). *Antioxid. Redox Signal.* **7**, 348–366.
Sturm, N., Jortzik, E., Mailu, B. M., Koncarevic, S., Deponte, M., Forchhammer, K., Rahlfs, S. & Becker, K. (2009). *PLoS Pathog.* **5**, e1000383.
Tripathi, T., Röseler, A., Rahlfs, S., Becker, K. & Bhakuni, V. (2010). *Biochimie*, **92**, 284–291.
Tsang, M. L. (1981). *J. Bacteriol.* **146**, 1059–1066.
Winn, M. D. *et al.* (2011). *Acta Cryst.* D**67**, 235–242.
Wong, J. H., Cai, N., Balmer, Y., Tanaka, C. K., Vensel, W. H., Hurkman, W. J. & Buchanan, B. B. (2004). *Phytochemistry*, **65**, 1629–1640.
Yu, J., Zhang, N.-N., Yin, P.-D., Cui, P.-X. & Zhou, C.-Z. (2008). *Proteins*, **72**, 1077–1083.
Zeldin, O. B., Gerstel, M. & Garman, E. F. (2013). *J. Appl. Cryst.* **46**, 1225–1230.